Journal of Solid State Chemistry 183 (2010) 1231–1238

Contents lists available at ScienceDirect

Journal of Solid State Chemistry

journal homepage: www.elsevier.com/locate/jssc

Structure and conductivity of strontium-doped cerium orthovanadates $Ce_{1-x}Sr_xVO_4$ $(0 \leq x \leq 0.175)$

Christophe T.G. Petit, Rong Lan, Peter I. Cowin, Shanwen Tao *

Department of Chemistry, Heriot-Watt University, Edinburgh EH14 4AS, UK

ARTICLE INFO

Article history:
Received 23 December 2009
Received in revised form
20 March 2010
Accepted 25 March 2010
Available online 30 March 2010

Keywords:
$Ce_{1-x}Sr_xVO_4$
Conductivity
Solid solution
Cerium orthovanadates

ABSTRACT

A-site substituted cerium orthovanadates, $Ce_{1-x}Sr_xVO_4$, were synthesised by solid-state reactions. It was found that the solid solution limit in $Ce_{1-x}Sr_xVO_4$ is at $x=0.175$. The crystal structure was analysed by X-ray diffraction and it exhibits a tetragonal zircon structure of space group $I4_1/amd$ (1 4 1) with $a=7.3670$ (3) and $c=6.4894$ (1) Å for $Ce_{0.825}Sr_{0.175}VO_4$. The UV–vis absorption spectra indicated that the compounds have band gaps at room temperature in the range 4.5–4.6 eV. Conductivity measurements were performed for the first time up to the strontium solid solution limit in air and in dry 5% H_2/Ar with conductivity values at 600 °C ranging from 0.3 to 30 mS cm^{-1} in air to 30–45 mS cm^{-1} in reduced atmosphere. Sample $Ce_{0.825}Sr_{0.175}VO_4$ is redox stable at a temperature below 600 °C although the conductivity is not high enough to be used as an electrode for solid oxide fuel cells.

1. Introduction

Rare-earth orthovanadates ($REVO_4$) were first studied in the 1950s as part of investigations to determine precise crystal structures [1], atomic arrangements in chemical series and ionic radius of crystals comprising heavy metals [2], and have been intensively studied in the last two decades, in particular lanthanoid orthovanadates ($LnVO_4$) due to the interesting physical properties exhibit by those compounds.

$REVO_4$ compounds exhibit an ABO_4 structure with two crystallisation types: tetragonal zircon [3] (naturally occuring in $ZrSiO_4$) and monoclinic monazite [4] (a phosphate mineral of rare-earth elements (REE)). In general, larger lanthanoid ions prefer the monazite type while smaller lanthanoids crystallise in the zircon type [5]. However, cerium (III) orthovanadate ($CeVO_4$), which according to phase diagrams is located at the boundary of zircon and monazite types, exhibit three polymorphic forms with the pseudo-octahedral looking-like structure of tetragonal scheelite (occuring naturally in calcium tungstate) in addition to the zircon and monazite type forms.

In the first studies of heavy metal orthovanadates ($HMVO_4$), researchers started to focus on crystal structures and group theory, looking for answers to explain the specific characteristics obtained when heavy metals and less generally *RE* elements of the *f*-block were mixed with orthovanadates. Based on a synthetic protocol previously established [6] (where ammonium metavanadate is mixed with the oxide or oxalate of a metal in order to obtain equimolar amounts of V_2O_5 and M_2O_3), Milligan and Vernon [1] reported structural studies on a group of fifteen $HMVO_4$ among which thirteen were lanthanoids; and demonstrated that the crystals had crystallised in body-centred tetragonal systems of space group $I4_1/amd$ (1 4 1).

A few years later, Carron et al. [2] pointed out that a correlation exist between ionic radii and the crystalline structures of *RE* vanadates, phosphates and arsenates. It was noted that for each series, boundaries between zircon-type structures (*Z*) and monazite-type structures (*M*) were identified at a specific element of the *RE* group, unique to each series. By comparing the size of the metals used in each series, investigations showed that a ratio of 1.86 is obtained between the cation (*M*) and the anion (oxygen) size limits that have been observed at (*Z*)–(*M*) structural boundaries.

In 1994, Chakoumakos et al. [5] followed the same path taken three decades earlier by Carron et al. [2] and managed to find relations between size limits and structures of $HMVO_4$–(*Z*) with *HM*=Sc, Y, Ce–Nd, Tb, Ho, Er–Lu. The high-quality powders of $HMVO_4$–(*Z*) were synthesised by homogeneous coprecipation in molten urea [7,8]. It was found that the average V–O bond lengths for all synthesised *HM* were similar with a small shortening with decreasing the atomic size of *HM*.

In more recent years, studies on members of the *RE* group were forsaken in bulk and attention was put onto specific orthovanadates or small groups of *RE* metals including La, Ce, Pr and Nd mostly. In 1995, Rao and Palanna [9] used the conventional solid-state ceramic technique to synthesise $CeVO_4$ and found that whereas $CeVO_4$ in itself is an insulator whether in pure or

* Corresponding author. Fax: +44 131 451 3180.
E-mail address: S.Tao@hw.ac.uk (S. Tao).

0022-4596/$ - see front matter © 2010 Elsevier Inc. All rights reserved.
doi:10.1016/j.jssc.2010.03.032

stoichiometric composition, a p-type semiconductive behaviour between room temperature and 800 °C was observed. The p-type conduction in the lattice was said to be the result of the coexistence of a few number of Ce^{4+} ions among the Ce^{3+} ions and therefore rendering the conduction via thermally activated motions of ions on equivalent sites.

Rao and Palanna's theory was however not supported by everyone as shown in two linked studies published in 1999 on the electrochemical character of $CeVO_4$, the first by Krasovec et al. [10] focussed on the cerium/vanadium oxide interface ion-storage films and the second by Picardi et al. [11]. Electrochemically speaking, it was found that $CeVO_4$ films behave in the same manner than crystalline V_2O_5 films. Electrochemical measurements could not however establish any contribution of redox processes involving cerium ions, agreeing with a structure of $CeVO_4$ containing only Ce^{3+} and V^{5+} ions.

In the last decade, doped $REVO_4$ have also being studied, in particular lanthanum and cerium orthovanadates doped with other *RE* [12] or with elements like calcium [13–18], iron [18–20] bismuth [13,14] or strontium [13,15–17] notably.

Firstly reported by Watanabe [13] with the study of highly conductive oxides, rapidly followed by the comparative study of Watanabe and Hirata [14] on calcium-doped and bismuth-doped cerium orthovanadates, $RE_{1-x}A_xVO_4$ species have attracted growing interest in the past years for their exceptional physical properties, among which a very high conductivity. Tsipis et al. [17] published in 2002 a study on the transport and physicochemical properties of *A*-substituted $CeVO_4$ with calcium ($x=0-0.2$) and strontium ($x=0.1$ only). Samples of calcium and strontium doped $CeVO_4$ were synthesised following a standard ceramic technique and XRD was used for verification of single zircon-type phases formation. The thermal expansions of the $Ce_{1-x}A_xVO_{4\pm\delta}$ were found to be almost linear for both doping agents in a range from 400 to 800 K.

A paper published a year after by the same group [16], focussed on the oxygen ionic conductivity of $Ce_{1-x}A_xVO_{4+\delta}$ (A=Ca, $x=0$–0.2; Sr $x=0.1$ only). Ionic conductivity and stability measurements were performed on oxygen in $Ce_{1-x}A_xVO_{4+\delta}$ and it was found that $Ce_{1-x}A_xVO_{4+\delta}-(Z)$ was stable in air up to 1300 K showing no phase transitions, and that the oxygen ionic conductivity was actually essentially independent of the concentration of the *A*-site dopant.

While the conductivity of $Ce_{0.9}Sr_{0.1}VO_4$ in air has been investigated, some aspects of strontium-doped cerium orthovanadates have yet still to be fully explored. The doping of cerium orthovanadates with strontium has shown to increase the conductivity of $CeVO_4$ with potential use as a redox stable anode for solid oxide fuel cells. To the best of our knowledge, the total conductivity of Sr-doped $CeVO_4$ in a reducing atmosphere has not been reported yet.

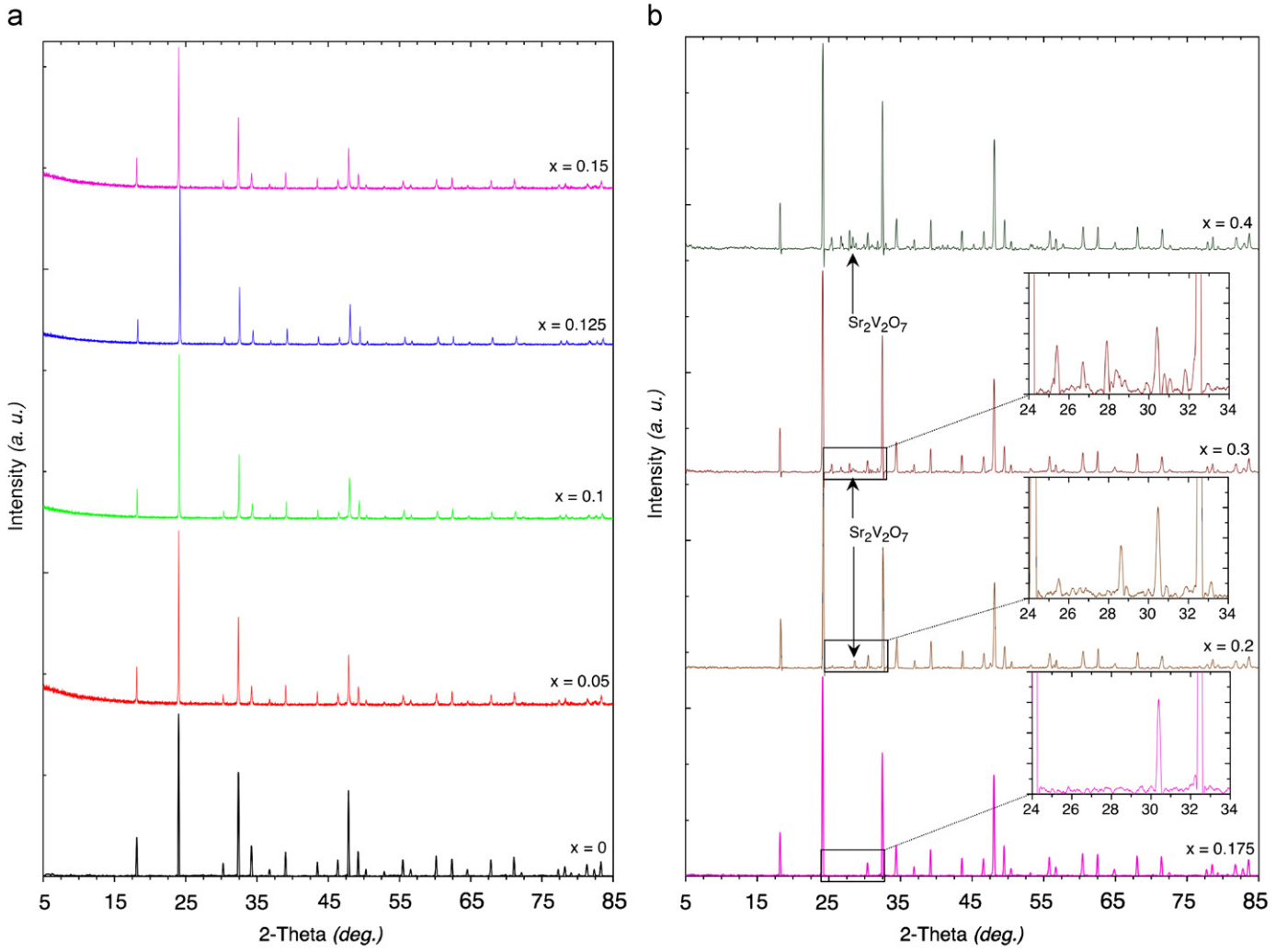

Fig. 1. (a) X-ray diffraction patterns of $Ce_{1-x}Sr_xVO_4$ with $0\le x\le 0.15$. (b) X-ray diffraction patterns of $Ce_{1-x}Sr_xVO_4$ with $0.175\le x\le 0.4$.

The aim of this study is therefore to have a systematic investigation of the phase (solid solution limit) and conductive behaviour in both air and 5%H_2/Ar of $Ce_{1-x}Sr_xVO_4$ compounds.

2. Experimental

2.1. Materials

CeO_2 (Alfa-Aesar, 99.9% REO), V_2O_5 (Aldrich, 99.6+% metals basis) and $SrCO_3$ (Aldrich, 99.95% metal basis) for the solid-state synthesis method were used as received.

2.2. Preparation

Pure, non-doped cerium orthovanadates were synthesised by a solid-state method using CeO_2 and V_2O_5 as cerium and vanadium sources. For the solid-state syntheses, stoichiometric amount of the respective oxides were fired at 800 °C at a heating rate of 5 °C min^{-1} for a dwelling time of 50 h. $Ce_{1-x}Sr_xVO_4$ compounds were synthesised by a solid-state method using CeO_2, V_2O_5 and $SrCO_3$ as cerium, vanadium and strontium sources. For the Sr-doping syntheses, stoichiometric amount of the respective oxides were fired at 950 °C at a heating rate of 5 °C min^{-1}, maintained for 66 h and cooled down to room temperature at the same rate of 5 °C min^{-1}. Powders were then regrounded and fired at 1000 °C at a heating rate of 5 °C min^{-1}, maintained for 72 h before being quenched. x was varied from 0.1 to 0.4 and a pure phase was obtained with $x \leq 0.175$.

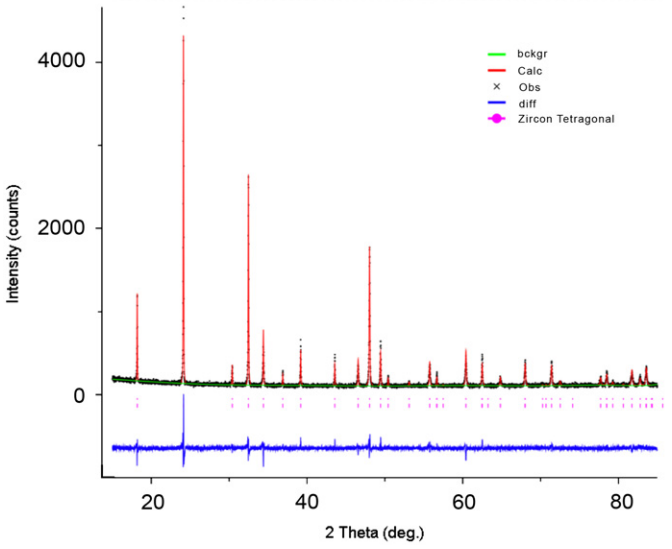

Fig. 2. Representation of an experimental (crossed) and calculated (solid line) X-ray diffraction profiles for $Ce_{0.825}Sr_{0.175}VO_4$. The difference profile is shown at the bottom of the profile.

2.3. Characterisation

2.3.1. UV–vis absorption

The band gaps at room temperature of all synthesised compounds were determined graphically from spectra obtained using a UV–vis spectrophotometer (Shimadzu UV-2550) operating with UVProbe® software.

2.3.2. X-ray powder diffraction

X-ray data were collected on a Bruker-AXS (D8 Advance) machine, controlled by DIFFRACT$^{plus\ TM}$, in the Bragg and Brentano reflection geometry with a Cu$K\alpha$ source, fitted with a LynxEye^{TM} detector. Absolute scans in the 2θ range 5–85° with step size of 0.009° and time step of 61.6 s were used during data collection.

2.4. Conductivity

Total conductivity measurements were carried out using a computer-controlled Solartron Analytical® SI 1260 impedance/gain phase analyser over a frequency range 1 MHz–0.01 Hz and a temperature range 600 °C to room temperature (~25 °C) and impedance data were recorded with the Solartron Impedance Measurement software, SMaRT^{TM}. Sample powders were pressed into pellets and sintered at temperatures depending on the sample themselves for 12 h (650 °C for $CeVO_4$, 900 °C for Sr-doped compounds). The relative densities of the samples were ~70–80%. Pellets were coated with silver paste for measurements in air and with platinum paste for measurements in a reduced atmosphere of 5% H_2/Ar dried through a solution of H_2SO_4 at 98%. Pellets coated with silver were directly fitted into the measuring apparatus while platinum coated samples were fired at 850 °C at a rate of 5 °C min^{-1}, dwelled for 2 h and then cooled down to room temperature before

Table 2
Average bond lengths, fraction of Ce^{4+} ions in $Ce_{1-x}Sr_xVO_4$ and oxygen hyperstoichiometry in $Ce_{1-x}Sr_xVO_4$ with $0 \leq x \leq 0.175$. (The Ce–O bond lengths were averaged between Ce–O1 and Ce–O2 interatomic distances.)

	$x=0$	$x=0.05$	$x=0.1$	$x=0.125$	$x=0.15$	$x=0.175$
Ce–O (Å)	2.4839	2.4825	2.4782	2.4773	2.4760	2.4758
V–O (Å)	1.7115	1.7105	1.7076	1.7071	1.7062	1.7060
ysp (%)	5.26 (1)	9.95 (2)	17.01 (4)	20.03 (3)	23.49 (5)	26.40 (3)
y_o (%)	5.26 (2)	9.45 (2)	15.32 (3)	17.53 (2)	19.97 (1)	21.78 (3)
δ	0.03 (4)	0.02 (2)	0.02(4)	0.01 (4)	0.01 (1)	0.02 (1)

Table 1
Crystallographic refinement parameters of $Ce_{1-x}Sr_xVO_4$ with $0 \leq x \leq 0.175$.

Crystallographic parameter	$CeVO_4$	$Ce_{0.95}Sr_{0.05}VO_4$	$Ce_{0.9}Sr_{0.1}VO_4$	$Ce_{0.875}Sr_{0.125}VO_4$	$Ce_{0.85}Sr_{0.15}VO_4$	$Ce_{0.825}Sr_{0.175}VO_4$
r Ln^{3+} (VIII) (Å)	1.143	1.143	1.143	1.143	1.143	1.143
λ (Å)	1.5418	1.5418	1.5418	1.5418	1.5418	1.5418
Crystal system	Tetragonal	Tetragonal	Tetragonal	Tetragonal	Tetragonal	Tetragonal
Space group	$I4_1/amd$	$I4_1/amd$	$I4_1/amd$	$I4_1/amd$	$I4_1/amd$	$I4_1/amd$
a (Å)	7.4004 (1)	7.3940 (1)	7.3779 (2)	7.3733 (1)	7.3690 (2)	7.3670 (3)
c (Å)	6.4982 (6)	6.4972 (2)	6.4905 (2)	6.4914 (2)	6.4886 (3)	6.4894 (1)
V (Å^3)	355.88 (5)	355.21 (3)	353.30 (1)	352.91 (1)	352.35 (1)|	352.20 (2)
ρ_{calc} (g cm^{-3})	4.7601	4.7200	4.6962	4.6767	4.6595	4.6367
Rp (%)	7.9	11.6	10.9	11.6	9.6	8.3
wRp (%)	10.0	14.8	13.8	14.9	12.8	10.6
χ^2	1.400	1.453	1.494	1.898	2.707	1.299

being used for pseudo 4-probe a.c. impedance measurements. Measurements in air were carried out on heating and those in reduced atmosphere on cooling after stabilisation was achieved. The sample dwelled at each temperature for at least 30 min to reach an equilibrium before conductivity measurements.

3. Results and discussion

3.1. Crystal structure

Single-phase powders of $Ce_{1-x}Sr_xVO_4$ were obtained up to $x=0.175$. Second phase $Sr_2V_2O_7$ was observed when $x>0.175$ (Fig. 1a and b). Rietveld refinements were carried out with both structural and profile parameters being varied. Initial structural and spatial parameters for the zircon structure were used as mentioned in the literature [5]. Wychoff sites assigned to Ce and Sr, V and O were 4*a*, 4*b* and 16*h*, respectively. Vanadium and oxygen were always considered – during the refinement processes – with full occupancies, whereas cerium and strontium occupancies were varied in accordance with the stoichiometry. Profile refinements were performed using GSAS [21]. The experimental and calculated profile for $Ce_{0.825}Sr_{0.175}VO_4$ is shown in Fig. 2. The refined parameters are listed in Table 1 for $Ce_{1-x}Sr_xVO_4$ and the average bond lengths in Table 2.

All single-phase powders obtained (up to the solid solution limit of $x=0.175$) exhibited a zircon tetragonal structure, crystallising in the space group $I4_1/amd$ (1 4 1). As shown in Table 1, the unit cell volume is decreasing as the dopant concentration is increased. Within the solid solution limit, both *a* and *c* are globally decreasing through the whole series (Fig. 3).

This latter behaviour can be explained by the distortions occurring as a consequence of the insertion of strontium ions. Indeed, Sr^{2+} ions are much larger than Ce^{3+} ions (1.40 and 1.143 Å, respectively) and this difference should influence the observed average bond lengths within the unit cell, but as shown in Table 2, Ce/Sr–O and V–O interatomic distances keep decreasing as the dopant concentration is increased.

While decreasing, V–O bond lengths still correlate with the ionic bond length of 4–2-coordinated V^{5+}–O^{2-} couple, whereas Ce/Sr–O bond lengths are not representative of the 8–2-coordinated Ce^{3+}/Sr^{2+}–O^{2-} couple. In fact, these are smaller than expected if it is considered that the insertion of larger ions into the lattice – where all cerium sites are occupied by Ce^{3+} ions – should increase the interatomic distances between cerium and oxygen. As this is obviously not the case, the possibility of the formation of Ce^{4+} ions to compensate the charge loss introduced by the insertion of a 2^+ ion may be considered.

By taking into account the average bond lengths of Ce–O as being an average of both Ce^{3+}–O^{2-} and Ce^{4+}–O^{2-} combinations, the fraction of Ce^{4+} ions present in each compound can be determined using Eqs. (1) and (2) with Eq. (1) giving the fraction of Ce^{4+} ions (y_{sp}) occupying Ce-site within the structure that are actually occupied by cerium atoms and Eq. (2) providing the overall fraction of Ce^{4+} ions (y_o) contained within each compound considering the total number of Ce-sites, even if some are in fact not occupied by cerium atoms

$$y_{sp}(\%)=\frac{\left[\frac{(Ce-O\ \text{b.l.})-(Sr^{2+}-O^{2-}\ \text{b.l.})\times x}{1-x}\right]-(Ce^{3+}-O^{2-}\ \text{b.l.})}{(Ce^{4+}-O^{2-}\ \text{b.l.})-(Ce^{3+}-O^{2-}\ \text{b.l.})}\times 100 \quad (1)$$

with (Ce–O b.l.) the average cerium–oxygen interatomic distances given in Table 2, $(Sr^{2+}$–O^{2-} b.l.$)=2.61$ Å, $(Ce^{3+}$–O^{2-} b.l.$)=2.493$ Å and $(Ce^{4+}$–O^{2-} b.l.$)=2.32$ Å extracted from a ionic radii database [22] which was originally reported by Shannon [23]

$$y_o(\%)=y_{sp}\times(1-x) \quad (2)$$

Mathematical demonstration for Eq. (1) is given in Appendix A.

After Ce^{4+} fractions are determined, the results can be used in the crystal electroneutrality law [17] in order to determine the

Table 3
Band gap energies of $Ce_{1-x}Sr_xVO_4$ with $0\le x\le 0.175$.

	Band gap energy (eV)
$CeVO_4$	4.635 (2)
$Ce_{0.95}Sr_{0.05}VO_4$	4.630 (1)
$Ce_{0.9}Sr_{0.1}VO_4$	4.615 (3)
$Ce_{0.875}Sr_{0.125}VO_4$	4.580 (4)
$Ce_{0.85}Sr_{0.15}VO_4$	4.590 (1)
$Ce_{0.825}Sr_{0.175}VO_4$	4.555 (3)

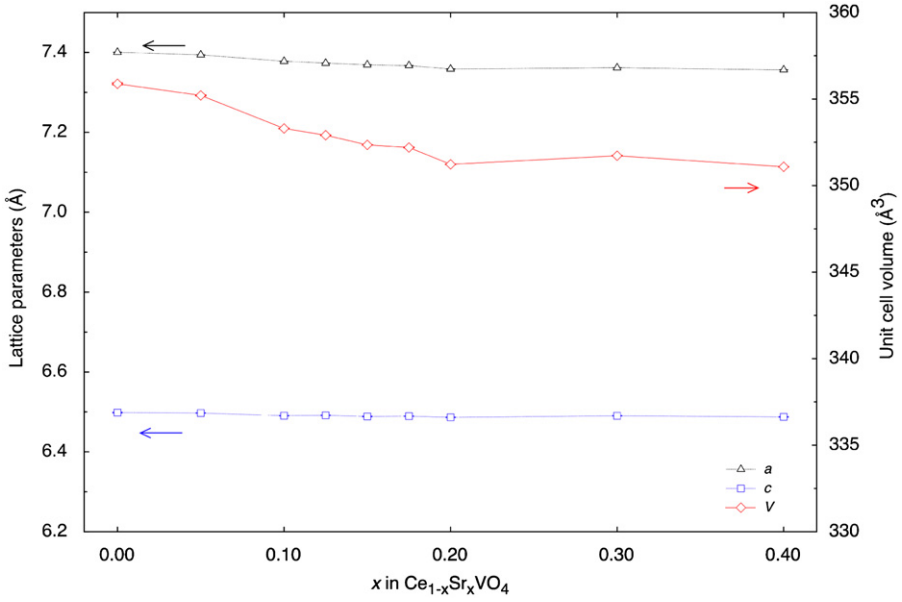

Fig. 3. Lattice parameters and volume reduction in $Ce_{1-x}Sr_xVO_4$ with $0\le x\le 0.4$.

hyperstoichiometric factor of oxygen δ within $(Ce^{3+}_{1-y}Ce^{4+}_{y})_{1-x}Sr_xVO_{4+\delta}$ using Eq. (3)

$$\delta = \frac{y_{sp} - x - xy_{sp}}{2} \quad (3)$$

As indicated in Table 2, the overall fraction of Ce^{4+} ions is comprised between 5% in non-doped cerium orthovanadate and just below 22% at the doping limit. It can also be noticed that the major increase is occurring from a state where the dopant is absent to a state where the dopant is added, at levels of 0.05 and 0.1. This kind of trend, suggestive of a plateau concentration of Ce^{4+} reflects on the variations of Ce/Sr–O bond lengths as well as on the variations of the lattice parameter *a*.

Values for the hyperstoichiometry of oxygen range from +0.03 to +0.01 indicating the presence of extra oxygen within the lattice (Table 2). Oxygen interstitials were also observed in a similar oxide $CeNbO_{4+\delta}$ [24]. It seems that more Ce^{4+} ions are formed for charge compensation when doped with strontium. The oxide tends to remain oxygen excess even after doping with strontium.

Concerning band gap energies, values were determined using Eq. (4) (Beer–Lambert inverse exponential power law) assuming

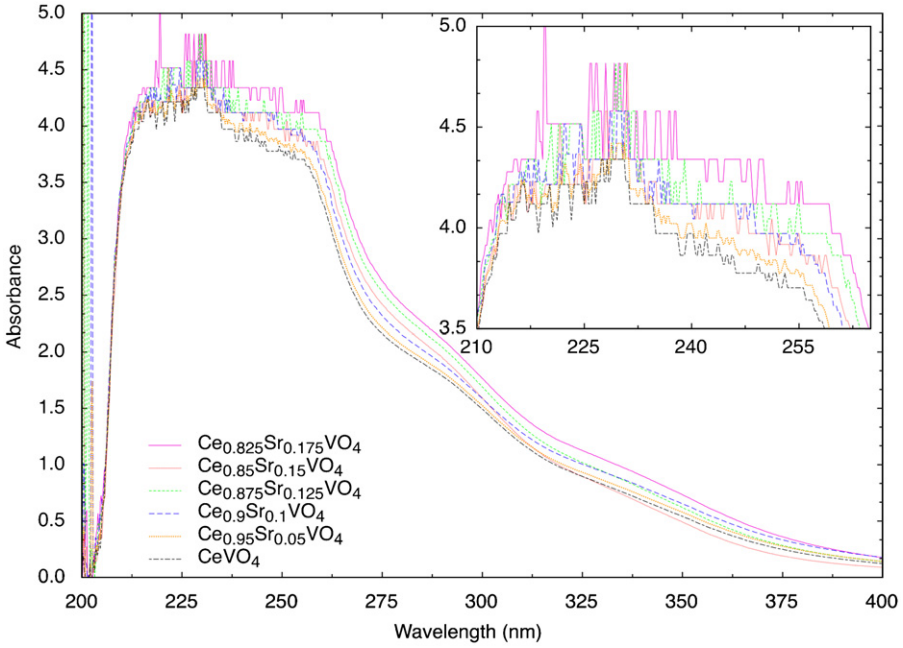

Fig. 4. UV–vis absorbance spectra of $Ce_{1-x}Sr_xVO_4$ with $0 \le x \le 0.175$.

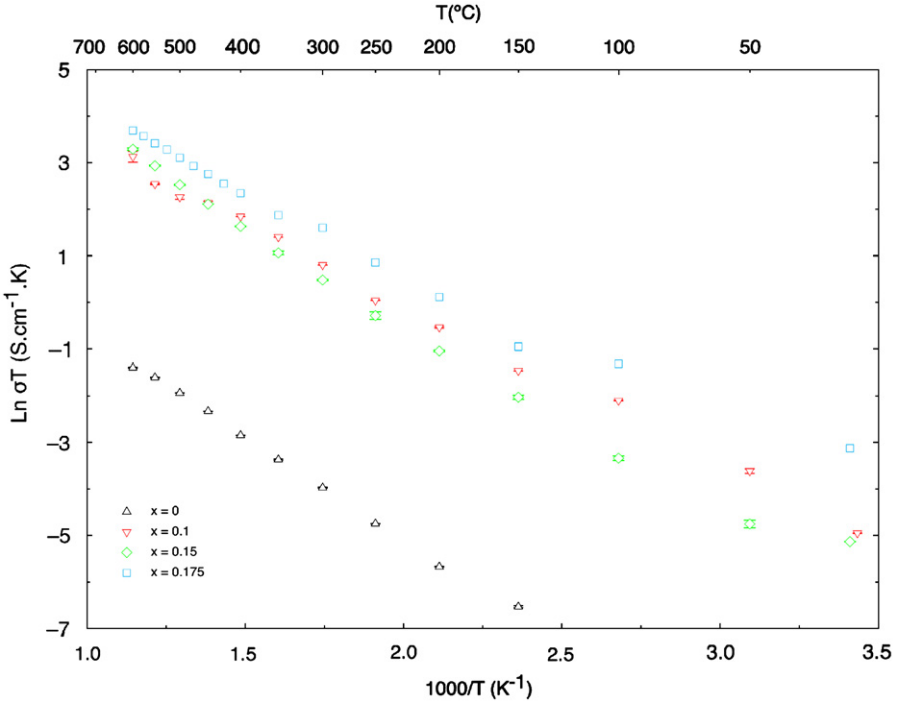

Fig. 5. Conductivity in air as a function of *x* in $Ce_{1-x}Sr_xVO_4$ with $0 \le x \le 0.175$.

Eq. (5), the absorption coefficient dependence on the energy level E

$$\alpha(E)_{\text{measured}} = -\frac{1}{d}\ln(\tau_{\text{normalised}}(E)) \quad (4)$$

with $\alpha(E)_{\text{measured}}$, the measured adsorption coefficient; d, the sample thickness and τ, the normalised transmittance energy

$$\alpha(E)_{\text{measured}} \propto \sqrt{E-E_g} \quad (5)$$

with E_g, the band gap energy.

If the measured absorption coefficient $\alpha(E)$ for an energy level E is proportional to the square-root of the difference between this energy and the band gap energy (E_g), the square-root dependence of $\alpha(E)$ on E would yield a linear dependence of $\alpha(E)^2$ on E.

As a result, a plot of $\alpha(E)^2$ against E would have a linear segment starting at the sample absorption edge. Extrapolating this segment to the abscise axis would give the value of the band gap energy for the considered sample. Results are given in Table 3 and the measured UV spectra in Fig. 4. More in details, solutions of known concentration were prepared for each sample represented in Fig. 4. UV scans were performed and data obtained were used to determine E_g through a multi-steps procedure involving conversion of absorbance into transmittance, normalisation, the determination of energy values in electron volt from the wavelengths, the calculation of $\alpha(E)$ and subsequently of $\alpha(E)^2$ from Eq. (4) and the extraction of the band gap energy values from the plots of $\alpha(E)^2$ against E.

The values obtained from the extrapolation – tabulated in Table 3 – show that at room temperature, $Ce_{1-x}Sr_xVO_4$ with $0 \le x \le 0.175$ compounds are insulators, as expected.

3.2. Conductivity

Values obtained from the conductivity measurements – performed in air and in dry 5% H_2/Ar – were used to plot Arrhenius type plots of the conductivity against inverse temperature. Activation energies and pre-exponential factors were extracted from the slopes and the intercepts of the fitted lines.

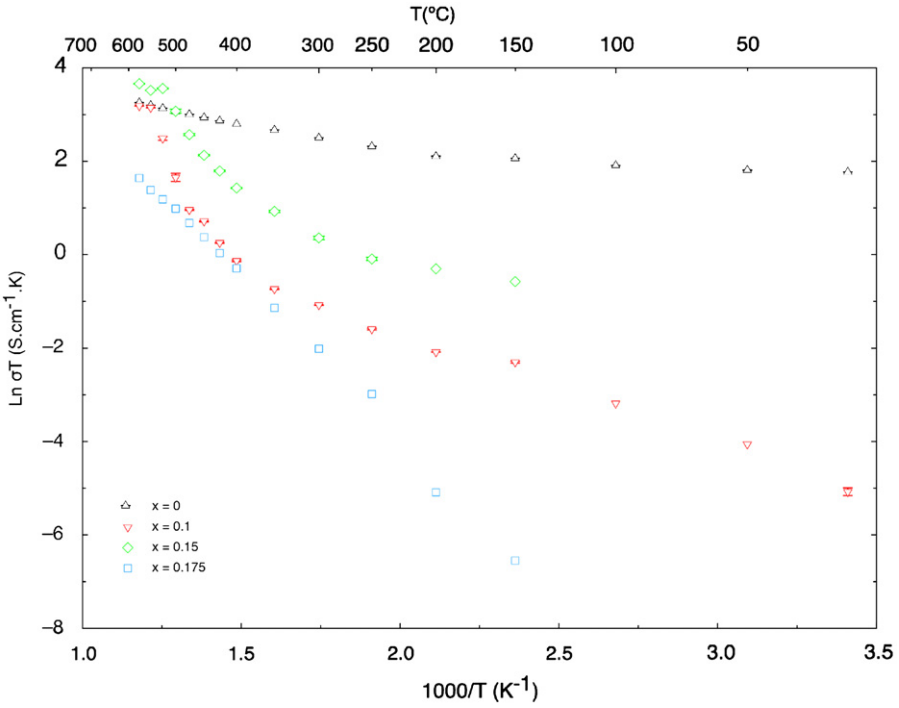

Fig. 6. Arrhenius plots of the conductivity in dry 5% H_2/Ar of $Ce_{1-x}Sr_xVO_4$ with $0 \le x \le 0.175$.

Table 4
Arrhenius constants of $Ce_{1-x}Sr_xVO_4$ with $0 \le x \le 0.175$.

E_a in kJ mol^{-1} A in S K cm^{-1}	$CeVO_4$	$Ce_{0.9}Sr_{0.1}VO_4$	$Ce_{0.85}Sr_{0.15}VO_4$	$Ce_{0.825}Sr_{0.175}VO_4$
Air				
E_a	36.3 ± 0.3	28.3 ± 0.4	32.3 ± 0.7	25.42 ± 0.2
A	38.4 ± 1.1	878.8 ± 0.4	1654.5 ± 1.2	1254.50 ± 1.0
Dry 5% H_2-Ar				
High temp.				
E_a	10.6 ± 0.2	115.2 ± 7.5	75.2 ± 6.5	49.2 ± 1.3
A	112.3 ± 1.0	$3.7.10^8$ ± 3.0	$2.4.10^6$ ± 2.8	$5.0.10^3$ ± 1.0
Low temp.				
E_a	2.3 ± 0.2	20.7 ± 0.7	12.4 ± 1.8	NA
A	14.8 ± 1.1	30.9 ± 1.2	17.7 ± 1.5	NA
Approx. temp. border (°C)	575	575	525	NA

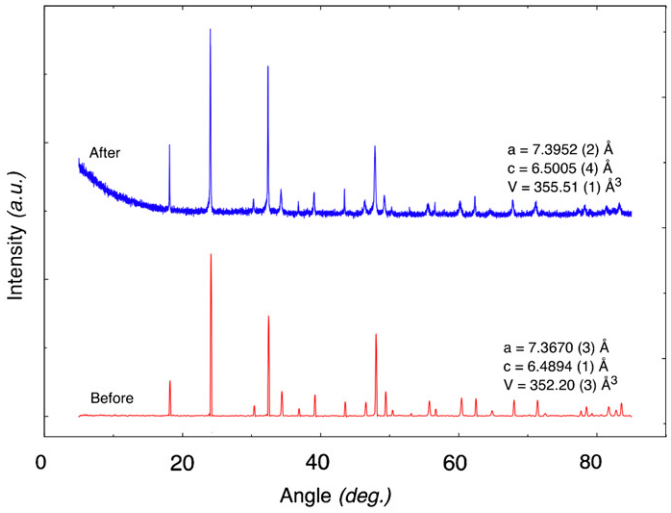

Fig. 7. X-ray diffraction pattern of $Ce_{0.825}Sr_{0.175}VO_4$ before and after conductivity measurement in dry 5% H_2/Ar.

Conductivity results expressed in the form of Arrhenius plots are shown in Figs. 5 and 6 for $Ce_{1-x}Sr_xVO_4$ compounds and the activation energies are listed in Table 4. It can be seen, referring to Fig. 5 that the doping of cerium orthovanadate with strontium improved the conductivity of the compounds in comparison with the non-doped sample. The increased conductivity in doped samples is related to smaller lattice parameters which makes the jumping of charge carriers much easier. The activation energies tabulated in Table 4 for samples in air were found to be equivalent, while still being lower for strontium-doped species than for non-doped $CeVO_4$. In our experiments, the conductivity of $CeVO_4$ and $Ce_{0.9}Sr_{0.1}VO_4$ is 2.8×10^{-4} and 2.9×10^{-2} S cm^{-1}, respectively, at 600 °C which are lower than those reported by Tsipis et al. [17], namely 2.0×10^{-2} and 0.1 S cm^{-1} for $CeVO_4$ and $Ce_{0.9}Sr_{0.1}VO_4$, respectively, under the same conditions. However, the apparent conduction activation energy for $CeVO_4$ of 36.3 ± 0.3 kJ mol^{-1} (Table 4) is very close to the reported 37.9 ± 0.01 kJ mol^{-1} [17] although the apparent conduction activation energy for $Ce_{0.9}Sr_{0.1}VO_4$ (28.3 ± 0.4 kJ mol^{-1}) is slightly lower than the reported 34.8 ± 0.5 kJ mol^{-1} [17]. The difference may be mainly related to the various measurement methods used. In our experiments, pseudo 4-probe a.c. impedance spectroscopy was used while 4-probe dc technique was used by Tsipis et al. [17].

Concerning measurements in dry 5% H_2/Ar, it can be observed in Fig. 6 that the general conductivity of doped $CeVO_4$ compounds were similar or increased; ranging from 30 to 45 mS cm^{-1} at reduced oxygen pressure compared to around 30 mS cm^{-1} in air. $CeVO_4$ maximum conductivity at 600 °C jumps from 0.3 to 30 mS cm^{-1} in air and in dry hydrogen atmosphere, respectively, indicating n-type conduction which could be related to the reduction of Ce^{4+} or/and V^{5+} ions. While the dopant concentration had little influence on the conductivity in air, it can be observed that in reduced atmosphere the higher the doping level, the lower the overall conductivity at a temperature below 500 °C. In comparison with values in air, the lower conductivity of Sr-doped $CeVO_4$ in a reducing atmosphere indicates that they could be p-type conductors at low pO_2, as it is the case in example for $CeNbO_{4+\delta}$ [24].

Samples within the solid solution limit are redox stable during the conductivity measurement in 5% H_2/Ar up to 600 °C. As shown in Fig. 7, XRD pattern of sample $Ce_{0.825}Sr_{0.175}VO_4$ is almost unchanged upon reduction and can be considered as being redox stable below 600 °C. The lattice expansion of sample $Ce_{0.825}Sr_{0.175}VO_4$ on reduction is believed to be due to the reduction of both cerium and vanadium ions because both the Ce–O and V–O bond lengths increased in the reduced sample. The bond lengths extracted from the pattern are 2.5248 Å for Ce–O (average) and 1.7309 Å for V–O compared with 2.4758 Å for Ce–O (average) and 1.7060 Å for V–O before the conductivity measurement. The values obtained for the activation energies for doped species in reduced atmosphere were lower at low temperatures and higher at high temperatures than in air. In comparison to $CeVO_4$, doped species activation energies were all higher, whether at low or high temperatures in accordance with an overall decreasing conductivity.

Another point worth noting is that variations in activation energies for doped compounds in reduced atmosphere reflect the observation made during conductivity measurements; namely that the dopant concentration has little effect on conductivity values in air, but does in reduced atmosphere. Indeed, variation percentages in reduced atmosphere are around 35–40% for high and low temperatures, respectively, whereas the difference in air is only about 12%.

4. Conclusion

Single phase powders of $Ce_{1-x}Sr_xVO_4$ with $0\le x\le0.175$ were synthesised by a standard ceramic technique. Second phase $Sr_2V_2O_7$ appeared when strontium doping level is greater than 0.175. All samples within the solid solution limit were found to exhibit the tetragonal zircon type structure of space group $I4_1/amd$ (1 4 1). Conductivity measurements carried out in air and in reduced atmosphere have shown that the conductivities of Sr-doped samples are higher in air but lower in dry 5%H_2/Ar. While $CeVO_4$ exhibits an increased conductivity in reduced atmosphere, the total conductivity of doped samples is decreasing indicating p-type conduction for Sr-doped $CeVO_4$ at lower pO_2. Sample $Ce_{0.825}Sr_{0.175}VO_4$ is redox stable at a temperature below 600 °C although some lattice expansion was observed which is related to the reduction of both cerium and vanadium ions.

Acknowledgments

We thank EPSRC for funding and Ms. Marian Millar for the powder XRD data collection. One of the authors (Petit) thanks Alexandra K. Stephenson for her advices on the crystal structures refinements.

Appendix A. Mathematical demonstration of Eq. (1)

The average bond lengths given in Table 2 correspond to the interatomic distances between cerium sites and oxygen sites, whether the former is occupied by cerium atoms or not, giving,

$$(\mathrm{Ce{-}O\ b.l.}) = x\times(\mathrm{Sr^{2+}{-}O^{2-}\ b.l.}) + (1-x)\times(\mathrm{Ce{-}O^{2-}\ b.l.})$$

Considering that the composition of calcium-doped cerium orthovanadates is as follow, $(Ce_y^{4+}Ce_{1-y}^{3+})_{1-x}Sr_xVO_4$, the previous equation can be rewritten as,

$$(\mathrm{Ce{-}O\ b.l.}) = x\times(\mathrm{Sr^{2+}{-}O^{2-}\ b.l.}) + (1-x)[y\times(\mathrm{Ce^{4+}{-}O^{2-}\ b.l.}) + (1-y)\times(\mathrm{Ce^{3+}{-}O^{2-}\ b.l.})]$$

Rearranging this latter to extract y,

$$\frac{(\mathrm{Ce{-}O\ b.l.}) - (\mathrm{Sr^{2+}{-}O^{2-}\ b.l.})\times x}{(1-x)} = [y\times(\mathrm{Ce^{4+}{-}O^{2-}b.l.}) + (\mathrm{Ce^{3+}{-}O^{2-}\ b.l.}) - y\times(\mathrm{Ce^{3+}{-}O^{2-}\ b.l.})]$$

$$\left[\frac{(\mathrm{Ce{-}O\ \ b.l.}){-}(\mathrm{Sr^{2+}{-}O^{2-}\ \ b.l.})\times x}{(1-x)}\right]-(\mathrm{Ce^{3+}{-}O^{2-}\ \ b.l.})=y \times[(\mathrm{Ce^{4+}{-}O^{2-}b.l.})+(\mathrm{Ce^{3+}{-}O^{2-}\ \ b.l.})]$$

$$\frac{\left[\frac{(\mathrm{Ce{-}O\ \ b.l.}){-}(\mathrm{Sr^{2+}{-}O^{2-}\ \ b.l.})\times x}{(1-x)}\right]-(\mathrm{Ce^{3+}{-}O^{2-}\ \ b.l.})}{[(\mathrm{Ce^{4+}{-}O^{2-}\ \ b.l.})+(\mathrm{Ce^{3+}{-}O^{2-}\ \ b.l.})]}=y$$

Leading to Eq. (1), once put into percent,

$$y_{sp}(\%)=\frac{\left[\frac{(\mathrm{Ce{-}O\ \ b.l.}){-}(\mathrm{Sr^{2+}{-}O^{2-}\ \ b.l.})\times x}{1-x}\right]-(\mathrm{Ce^{3+}{-}O^{2-}\ \ b.l.})}{(\mathrm{Ce^{4+}{-}O^{2-}\ \ b.l.}){-}(\mathrm{Ce^{3+}{-}O^{2-}\ \ b.l.})]}\times 100$$

Appendix B. Supplementary material

Supplementary data associated with this article can be found in the online version at doi:10.1016/j.jssc.2010.03.032.

References

[1] W.O. Milligan, L.W. Vernon, J. Phys. Chem. 56 (1952) 145.
[2] M.K. Carron, M.E. Mrose, K.J. Murata, Am. Mineral. 43 (1958) 985.
[3] H. Fuess, A. Kallel, J. Solid State Chem. 5 (1972) 11.
[4] C.E. Rice, W.R. Robinson, Acta Cryst. B 32 (1976) 2232.
[5] B.C. Chakoumakos, M.M. Abraham, L.A. Boatner, J. Solid State Chem. 109 (1994) 197.
[6] W.O. Milligan, L.M. Watt, H.H. Rachford, J. Phys. Colloid Chem. 53 (1949) 227.
[7] M.M. Abraham, L.A. Boatner, T.C. Quinby, D.K. Thomas, M. Rappaz, Radioactive Waste Manage. 1 (1980) 181.
[8] B.C. Sales, L.A. Boatner, Radioactive waste forms for the future, in: W. Lutze, R.C. Ewing (Eds.), Elsevier, New-York, 1988, p. 507.
[9] I.S. Rao, O.G. Palanna, Bull. Mater. Sci. 18 (1995) 593.
[10] U.O. Krasovec, B. Orel, A. Surca, N. Bukovec, R. Reisfeld, Solid State Ionics 118 (1999) 195.
[11] G. Picardi, F. Varsano, F. Decker, U.O. Krasovec, B. Orel, A. Surca, Electrochem. Acta 44 (1999) 3157.
[12] S. Varma, B.N. Wani, N.M. Gupta, Mater. Res. Bull. 37 (2002) 2117.
[13] A. Watanabe, J. Solid State Chem. 153 (2000) 174.
[14] T. Hirata, A. Watanabe, J. Solid State Chem. 158 (2001) 264.
[15] E.V. Tsipis, V.V. Kharton, J.R. Frade, J. Eur. Ceram. Soc. 25 (2005) 2623.
[16] E.V. Tsipis, V.V. Kharton, N.P. Vyshatko, A.L. Shaula, J.R. Frade, J. Solid State Chem. 176 (2003) 47.
[17] E.V. Tsipis, M.V. Patrakeev, V.V. Kharton, N.P. Vyshatko, J.R. Frade, J. Mater. Chem. 12 (2002) 3738.
[18] S. Mahapatra, R. Vinu, D. Saha, T.N.G. Row, G. Madras, Appl. Catal. A 361 (2009) 32.
[19] S. Varma, B.N. Wani, N.M. Gupta, Appl. Catal. A 241 (2003) 341.
[20] S. Varma, B.N. Wani, A. Sathyamoorthy, N.M. Gupta, J. Phys. Chem. Solids 65 (2004) 1291.
[21] A.C. Larson, R.B. Von Dreele, General Structure Analysis System (GSAS), 2004, Los Alamos National Laboratory Report, LAUR, 86.
[22] CrystalMaker®, A crystal and molecular structures program for Mac and Windows, 1994–2009, CrystalMaker Software Ltd., Oxford, England, ⟨www.crystalmaker.com⟩.
[23] R.D. Shannon, C.T. Prewitt, Acta Cryst. B 25 (1969) 925–946.
[24] E.V. Tsipis, C.N. Munnings, V.V. Kharton, S.J. Skinner, J.R. Frade, Solid State Ionics 177 (2006) 1015.